Journal of Energy Storage 45 (2022) 103495

Contents lists available at ScienceDirect

Journal of Energy Storage

journal homepage: www.elsevier.com/locate/est

Research Papers

Optimization of the thermal storage system in a solar-driven refrigeration system equipped with an adjustable jet-ejector

José Manuel Luján, José Galindo, Vicente Dolz *, Alberto Ponce-Mora

CMT – Motores Térmicos, Universitat Politècnica de València, 46022, Spain

ARTICLE INFO

Keywords:
Solar refrigeration
System sizing
Hot thermal storage system
Adjustable jet-ejector
Dynamic behavior
Thermal management

ABSTRACT

The present paper shows a numerical research about the influence of different thermal storage capacities and thermal power consumption strategies in a solar-driven air-conditioning system operating with refrigerant R1234yf. The computational model is fed with hourly climatic data (solar irradiance and ambient temperature) of the typical meteorological year of a Mediterranean location. A special focus is put on the dynamic response of the refrigeration system, the solar collector, and the sensible heat storage tank. Since the refrigeration needs are nearly synchronized with the sunny hours, small tank volumes are the most convenient architecture to achieve a rapid heating-up after tank discharges. For a parabolic trough collector span of 7.1 m, 13.3 kW of thermal power consumption represents a reasonable trade-off between the main performance indicators, mainly, the refrigeration capacity, COP_{th} (thermal coefficient of performance) and the system's capability to operate properly ensuring an adequate thermal level in the heat reservoir.

1. Introduction

The development and implementation of solar-driven refrigeration technologies might contribute to achieving significant primary energy savings in households, offices, and numerous industries [1,2]. The use of thermal storage systems in solar-driven machines is essential to cope with the intermittent nature of solar irradiance and contribute to a continuous system operation [3–5]. Depending on the heat storage principle the thermal storage system can be classified as:

- Sensible heat storage systems, in which the thermal power coming from the solar collector is used to raise the temperature of a liquid or solid (water, thermal oil, molten salt, rock, sand…). This technology is frequently implemented due to its low cost and the use of materials with low toxicity [6].
- Latent heat storage systems, in which phase transition in storage material occurs. The main advantage of using phase change materials (PCM) is the high-energy storage density at a nearly constant temperature [7–9].
- Thermochemical storage systems, which are based on reversible exothermic/endothermic chemical reactions. Despite their higher complexity and cost, this storage method is characterized by its compactness, high storage density, low heat losses, and long availability [10].

Based on the temperature gradient in the storage medium, the thermal storage systems can be also divided into thermally stratified and thermally mixed. The stratification is usually preferred due to its positive effect on solar collector efficiency [10].

The most convenient thermal storage system design in solar-powered refrigeration facilities is strongly influenced by the application and the operational requirements. There is not a clear consensus in the literature about the most appropriate design strategies. Sparber et al. [11] analyzed pilot solar cooling installations and pointed out the necessity of standardization rules in the storage system sizing. A high variability while selecting the most adequate storage system size in relation to the solar collector surface has been observed. This variability in the design criteria is reflected in the specialized literature and evidences the significance of the subject as well as the need of generating robust methodologies for adequate sizing.

For a solar-driven jet-ejector refrigeration system working under dynamic conditions, Tashtoush et al. [12] found that a thermal storage tank of 2 m^3 facilitates thermal stability and steady operation considering an evacuated tube collector area of 60m^2 and a targeted refrigeration capacity of 7 kW. Rosiek and Batlles [13] analyzed a single-effect solar-powered absorption machine equipped with flat plate collectors

* Corresponding author.
E-mail address: vidolrui@mot.upv.es (V. Dolz).

https://doi.org/10.1016/j.est.2021.103495
Received 16 June 2021; Received in revised form 21 October 2021; Accepted 25 October 2021
Available online 10 November 2021

Nomenclature

Acronyms

AJE	adjustable jet-ejector
ARS	adjustable refrigeration system
AR	jet-ejector area ratio
CFD	computational fluid dynamics
COP	coefficient of performance
DNI	direct normal irradiance
HTF	heat transfer fluid
PTC	parabolic trough collector
SP	spindle position
TMY	typical meteorological year
TSS	thermal storage system

Notation, Latin

A	area [m^2]
h	specific enthalpy [J/kg]
$\dot{m}$	mass flow rate [kg/s]
$\dot{Q}$	heat exchanger power [kW]
T	temperature [$^{\circ}C$]
V	volume [m^3]

Greek letters

ω	jet-ejector entrainment ratio [-]

Subscripts

amb	ambient
cl	cooling load
co	condenser/condensing conditions
ev	evaporator
ge	generator
HTF	heat transfer fluid
in	inlet
mf	jet-ejector mixed flow
out	outlet
pf	jet-ejector primary flow
PTC	parabolic Trough Collector
ref	reference situation/condition
sf	jet-ejector secondary flow
th	thermal
TSS	thermal storage system

(approximately 160 m^2) designed for a rated refrigeration capacity of 40 kW. They found that the usage of two water storage tanks with a capacity of 5000 l each is very important to maintaining the operation with irregular solar irradiance as well as providing an adequate thermal level in the morning early hours. Qu et al. [14] analyzed the dynamic behavior of a double effect absorption machine operating with a parabolic trough collector area of 52 m^2 and a rated refrigeration capacity of 16 kW. They stated that small thermal storage sizes are preferred (optimum of 4 m^3) in the cooling mode since solar irradiance and cooling demands nearly coincide. Syed et al. [15] investigated the dynamic behavior of a single effect absorption system that reached a maximum refrigeration capacity of 7.5 kW and was powered by 49.9 m^2 of flat plate collector modules. The refrigeration system was fitted with a hot thermal storage system of 2 m^3 which was able to avoid the cycling phenomena and was able to prolong the daily cooling period. More recently, Van Nguyen et al. [16] studied the dynamic response of a variable-geometry solar-driven jet-ejector refrigeration system with a rated refrigeration capacity of 1.5 kW, a thermal storage tank of 50 l, and four evacuated tube collectors with a total absorber area of 13 m^2. Their research work revealed that the storage tank was an effective auxiliary device capable of prolonging about 20 min the system operation with the absence or insufficient solar irradiance. The above-mentioned research works highlight the importance of a thermal storage system acting as a backup. An adequate sizing according to the installation characteristics is also crucial for an efficient operation.

Traditionally, jet-ejector refrigeration systems have received less attention in solar refrigeration applications than sorption systems due to their lower COP [17] and the incapacity showed by the baseline cycle architecture to operate robustly in off-design situations, which are, however, frequent in a standard operation. Nevertheless, they present low mechanical complexity, cost, and maintenance needs [18]. The adoption of advanced strategies like thermal storage systems [12,16,19,20], adjustable-geometry jet-ejectors [16,21–24], multiejector systems [25,26], or a combination of these technical solutions might allow greater flexibility and could open the way for a cost-competitive refrigeration system.

The main novelty of the present paper is the introduction of a systematic approach to determine the optimum sizing of a hot thermal storage tank according to the rated thermal power demands in an adjustable jet-ejector refrigeration system. The conclusions, however, could be extended to other solar-powered thermodynamic cycles with sensible heat thermal storage systems driven by a hot source with a comparable thermal level. The methodology described contemplates those situations in which the system operation is interrupted due to insufficient irradiance supply and intensive utilization of the heat reservoir. The ability of the system to remain in operation as well as its efficiency is directly related to the storage tank size and the nominal power extracted from the tank. The results are analyzed paying special attention to both the instantaneous response under particular and random climatic events as well as averaged representative values along an overall warm month.

The objective of the present investigation is to determine the optimum sizing of a small-scale solar-driven jet-ejector refrigeration system working under dynamic climatic conditions. For a fixed parabolic trough collector size, the influence of (i) the hot thermal storage tank volume and (ii) the nominal thermal power extracted from the tank, closely related to the jet-ejector sizing and the attainable refrigeration capacity, are evaluated paying special attention to their impact on the main performance indicators. For the reference parabolic trough collector span proposed in the present investigation, the most convenient storage tank size and power consumption strategy are found. The main findings and trends have later been corroborated with other PTC spans.

2. Description of the refrigeration system

The adjustable solar-driven jet-ejector refrigeration system (ARS) depicted in Fig. 1 uses the solar energy captured by the collector to evaporate a refrigerant at high pressure. On the solar field side, the system is equipped with a parabolic trough collector (PTC) acting as a solar concentrator and a thermal storage system (TSS) intended to accumulate thermal energy. The TSS of the ARS serves as a heat reservoir and its objective is to drive the ARS in absence of solar irradiance or start-up events. The ARS incorporates a sensible heat storage tank, which is the most commonly used storage device in thermally driven cooling applications [10].

The decision of selecting a sensible heat storage system is mainly sustained on its reduced cost when compared to PCMs [6] and also on its simplicity [3]. According to Sarbu and Sebarcievici [6], the cost of a complete sensible heat storage system ranges between 0.1 and 10 €/kWh while in the case of a latent heat storage system the cost oscillates between 10 and 50 €/kWh. Sensible heat storage systems would be the best option if priority is given to a low-cost implementation.

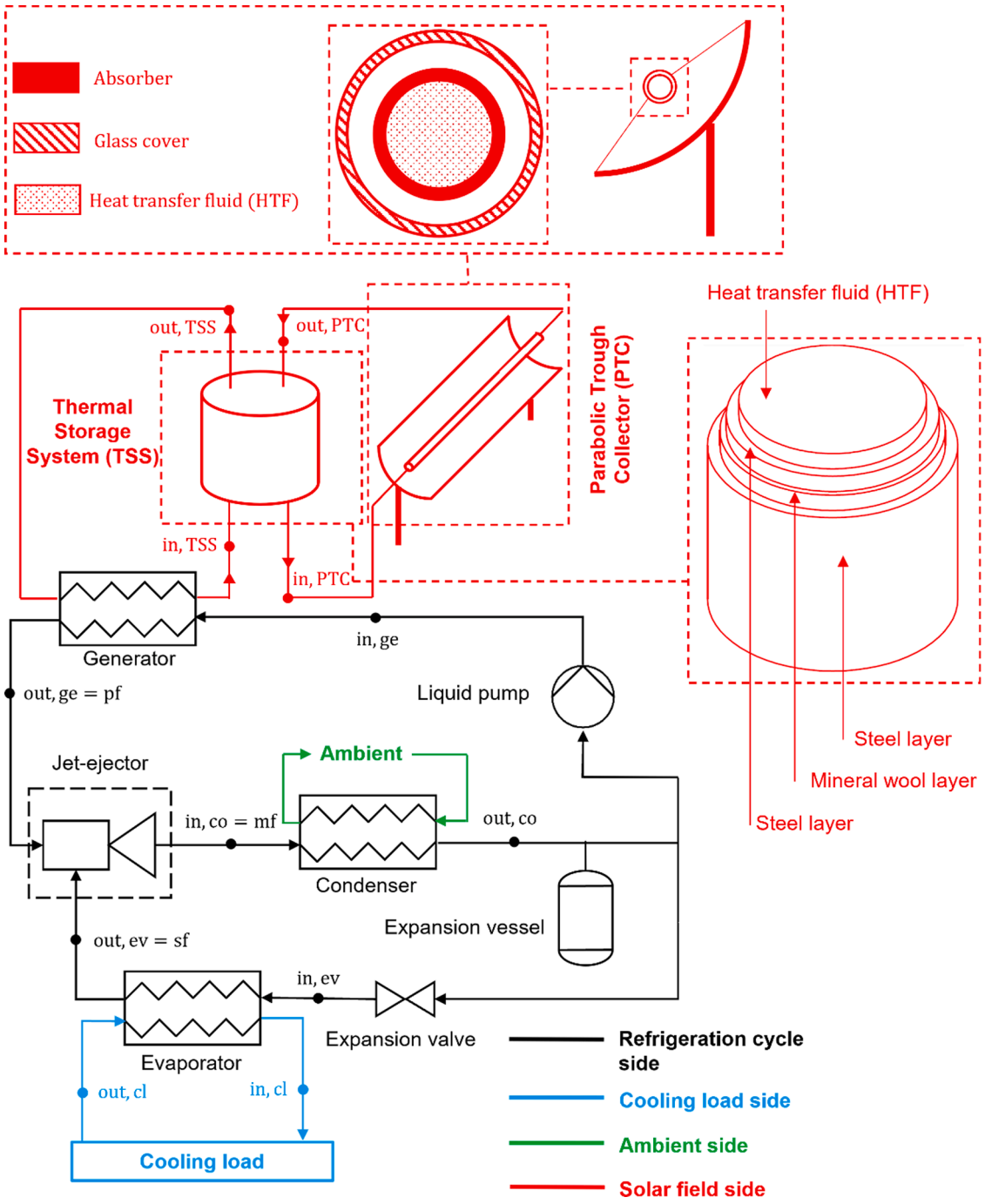

Fig. 1. Solar-driven jet-ejector refrigeration system with storage tank.

The heat power is accumulated in a cylindrical thermally mixed storage system in the form of sensible heat after passing through the PTC. The storage system jacket is composed of two structural steel layers of 1 cm separated by a mineral wool layer of 3 cm. The pumping system of the TSS recirculates the thermal oil towards the refrigeration system when the thermal level is sufficient ($T_{TSS} > 120^{\circ}C$) and the threshold outdoor temperature ($25^{\circ}C$) is exceeded. Otherwise, the absorbed solar irradiance is dedicated to raising the TSS internal temperature.

On the refrigeration system side, the jet-ejector acts as a passive device that produces a pressure lift in the secondary flow once it is mixed with the high-pressure stream. The resulting mixed flow at an intermediate pressure is condensed in a heat exchanger. A fraction of it passes through an expansion valve and then produces the desired refrigerating effect as the working fluid is evaporated in a heat exchanger (evaporator). In this heat exchange process heat is removed from the space with refrigeration needs. The new generation and environmentally friendly refrigerant R1234yf has been selected because of its low ecological impact and its moderate operating pressures in the generator, condenser, and evaporator. As demonstrated by the authors in prior research works [27], the response of the jet-ejector refrigeration system could be almost insensitive to the refrigerant selection if the jet-ejector internal shape is thoroughly optimized for given boundary conditions. The present research work considers a highly optimized jet-ejector design for the refrigerant R1234yf but, in accordance with the previous findings, very similar results could be expected if the same procedure is reproduced with other environmentally benign refrigerants

like R600a or R1234ze.

The jet-ejector entrainment ratio (ω), defined as the ratio between the secondary and primary mass flow rates ($\omega = \dot{m}_{sf}/\dot{m}_{pf}$,) governs the refrigeration system efficiency. An optimized entrainment ratio is crucial to achieving a cost-competitive system; it strongly depends on the jet-ejector internal geometry and the overall system operating conditions.

The thermal coefficient of performance, defined in Eq. (1), is usually designated as the main performance indicator of the thermally driven refrigeration system and it depends on the jet-ejector entrainment ratio. Considering a fixed-geometry jet-ejector, i.e., a device with no adaptation capabilities, the entrainment ratio (ω) and COP_{th} might be severely degraded when the system operates away from its design conditions.

$$COP_{th} = \omega \cdot \frac{h_{out,ev} - h_{in,ev}}{h_{out,ge} - h_{in,ge}} \quad (1)$$

A jet-ejector design with an adjustable spindle (see Fig. 2) is a useful mechanism to address this limitation. The adjustable jet-ejector (AJE) postulated in the present research is fitted with a spindle that is automatically displaced according to the instantaneous condensing temperature to maximize the AJE entrainment ratio. The spindle is moved when the refrigeration system operates away from its reference design condensing temperature (see Fig. 2) to an optimum position that is determined beforehand for each condensing temperature. This mechanism aims to tune in real-time the jet-ejector internal geometry, specifically the primary nozzle throat section, to guarantee an optimum jet-ejector area ratio (AR), defined as the ratio between the jet-ejector mixing chamber area and the primary nozzle throat area. This adaptive capacity enlarges the operative range of a fixed-geometry jet-ejector avoiding a drastic entrainment ratio drop beyond the critical condensing temperature. Likewise, the adjustable configuration improves the entrainment ratio when the jet-ejector operates below its critical condensing temperature. This is not the case of a constant-geometry jet-ejector; below its critical condensing temperature, its entrainment ratio remains unchanged.

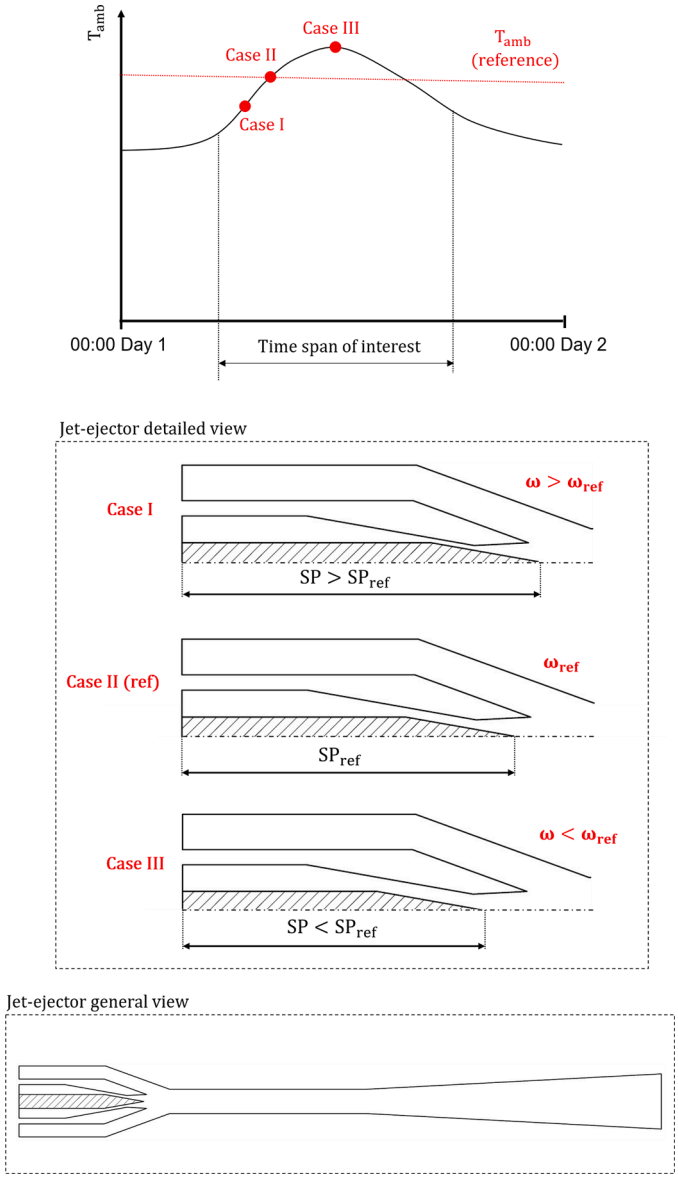

Fig. 2. Qualitative representation of the spindle optimum positioning (SP) inside the jet-ejector as a function of the ambient temperature and its influence over entrainment ratio (cross-sectional symmetric view).

The so-called operating envelope of the adjustable jet-ejector is formed by the entrainment ratio at the critical condition for different condensing temperatures and has been widely studied by some authors [21,28,29].

To design a robust and versatile refrigeration system special attention must be paid to the jet-ejector performance. Its key internal geometric dimensions, namely, the primary nozzle exit diameter, the nozzle exit position, and the mixing chamber diameter have been subject to a detailed optimization, together with an adequate selection of the suction chamber convergence angle, the diffuser divergence angle, and the primary nozzle divergence angle to avoid flow separation. For further details about the optimization process, the reader is referred to preceding research works [27,28]. The aim is to optimize its performance in its most representative operating scenario. These reference conditions are listed below:

- An evaporating temperature of 13 °C, which is compatible with air-conditioning applications [21,30]. The evaporating temperature target is assumed to be constant during all the studies and simulations.
- A condensing temperature of 40 °C, which is representative of the condensing temperature expected during the warmest days of the summer in Mediterranean locations. The condensing temperature, however, varies accordingly with the ambient temperature. Away from the reference condensing temperature the spindle displacement law would maintain acceptable performance.

The optimum jet-ejector, the result of the optimization process implemented in CFD, has a mixing chamber diameter of 3.7 mm, a nozzle exit position length of 3.5 mm, a nozzle exit diameter of 2.1 mm, a mixing chamber length of 45 mm, a diffuser length of 30 mm and a nozzle throat section of 1.88 mm^2, defined as an annular section when the spindle length (SP_{ref}) measures 13 mm. For more concrete details about the jet-ejector internal shape, the reader should refer to prior research works [28], where the internal contour is defined with a high level of detail.

The reference jet-ejector size is the optimum for a thermal power consumption of 4.4 kW at the reference (nominal) operating conditions, that is, $T_{co} = 40^{\circ}C$ and $T_{ev} = 13^{\circ}C$. To meet the thermal power consumptions established in the sensitivity analysis, which are different from the reference one, the reference jet-ejector should be scaled accordingly, however, its response and non-dimensional maps would not be altered.

3. Definition of performance indicators and manipulable variables

The influence of the TSS configuration over the ARS performance, which is the objective of the present investigation, is going to be assessed by monitoring three competing performance parameters:

I *Activation percentage*: The refrigeration system is intended to be activated in the time slot between 08:00 and 19:00 if the ambient temperature is above 25 °C. The activation percentage is defined as the time fraction in which the system can operate under the previous condition, that is, the time fraction between 08:00–19:00 with an ambient temperature above 25 °C in which the TSS has enough thermal level to drive the refrigeration system. An activation percentage of 100% would be the most desirable scenario and it would mean that the system has been able to operate all the time with refrigeration needs.

II *Refrigeration capacity* (Eq. (2)): Thermal power extracted from the indoor refrigerated space.

$$\dot{Q}_{ev} = \dot{m}_{sf} \cdot \left(h_{out,ev} - h_{in,ev}\right) \tag{2}$$

III *Thermal coefficient of performance* (COP_{th}), already presented in Eq. (1).

Three design parameters of the TSS are explored in a sensitivity study to maximize the activation percentage, refrigeration capacity and COP_{th}:

I *Thermal storage tank volume factor (f)*, which is presented in Eq. (3) and is defined as the ratio between the TSS volume and the solar collector surface [31]:

$$f = \frac{V_{TSS}}{A_{PTC}} \tag{3}$$

For a fixed collector surface, it is directly related to the TSS volume and informs about the storage system size in relation to the solar collector size. In the sensitivity study of the present investigation, the volume factor (f) varies between 0.02 m and 0.14 m. Higher volume factors denote higher storage capacities but also higher thermal inertia to heat the thermal oil contained in the TSS.

II *Nominal thermal power extracted from the thermal storage system* ($\dot{Q}_{ge}$), which is expressed in Eq. (4):

$$\dot{Q}_{ge} = \dot{m}_{pf} \cdot \left(h_{out,ge} - h_{in,ge}\right) \tag{4}$$

The definition of nominal thermal power corresponds with the thermal power consumed from the TSS at the reference (nominal) operating conditions, that is, $T_{co} = 40°C$ and $T_{ev} = 13°C$. Since the instantaneous variations in the condensing conditions govern the jet-ejector spindle positioning (SP), the nominal power extracted from the tank is directly related to the jet-ejector scalability (Fig. 3). The higher the nominal $\dot{Q}_{ge}$ the larger the jet-ejector should be to entrain more mass flow rate. Hence, the jet-ejector size selection predetermines the thermal power profile consumed from the TSS as illustrated in Fig. 3. The selection of a particular jet-ejector size will strongly influence the overall system performance, and an optimum size would exist depending on the designer's list of priorities. This choice significantly affects the system's thermal management of the heat reservoir.

The nominal thermal power is varied in the parametric study between 5 kW and 30 kW. A priori, the higher the nominal thermal power extracted from the tank, the higher the refrigeration capacity but, at the same time, the faster the energy stored in the TSS is consumed. Inappropriate management of the TSS energy consumption rate would result in time slots with refrigeration needs in which the system is unable to operate due to insufficient temperature in the TSS.

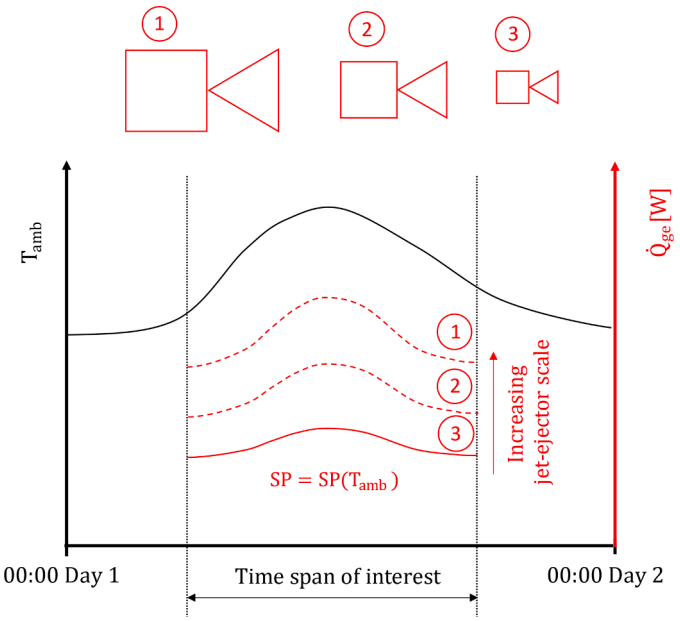

Fig. 3. Thermal power consumption from the TSS for different jet-ejector scales.

III *PTC span* (L_{PTC}), which is defined as the length of the PTC receiver. This parameter allows to modify the size of the solar field independently and, equivalently, the thermal power supplied to the TSS. The receiver length has been varied in the analysis between 5 m and 9 m.

4. Description of the computational models and validation

4.1. Computational models

The computational models used in the present investigation have been described in detail in prior research works [27,28] and are intended to model the thermal energy collecting system (elements marked in red color in Fig. 1) and the refrigeration machine subsystem (elements marked in black color in Fig. 1). Below, the modeling approach for each subsystem of the ARS and the main hypothesis adopted are summarized. The computational models are fed with the instantaneous evolution of the Direct Solar Irradiance (DNI) and ambient temperature during the warm months of the Typical Meteorological Year (TMY) in the geographical area of Valencia (Spain).

- *Adjustable refrigeration system (ARS)*: The model aims to compute the instantaneous COP_{th}, refrigeration capacity ($\dot{Q}_{ev}$) and activation percentage as a function of the instantaneous TSS thermal level, ambient temperature, and solar irradiance. The modeling technique is based on energy and mass conservation equations in the heat exchangers, the expansion valve, the jet-ejector, and the pump. The list of equations describing the refrigeration system behavior is described in detail in the literature [27,28,32].

  The efficiency of the ARS is calculated guaranteeing a minimum pinch point of 7 °C in all the heat exchangers and some degree of vapor superheating to avoid two-phase flow as the flow expands in the AJE primary nozzle. To simplify the calculation, pressure and thermal losses are neglected in all the conduction lines and heat exchangers.

- *Adjustable jet-ejector (AJE)*: The objective of this model is to determine the entrainment ratio (ω) of the AJE for multiple spindle positions and condensing temperatures: $\omega = \omega(T_{co}, SP)$ and transfer this

information to the ARS model to estimate the mass flow rate passing through the system and the refrigeration capacity. Eq. (5) comes from the research work of Galindo et al. [28] and describes the AJE performance envelope, that is, the optimum AJE entrainment ratio found at the critical condition. The optimum spindle positioning defines the AJE operating envelope and has been found by determining the entrainment ratio at the critical condensing temperature for multiple discrete spindle positions as depicted in Fig. 4. Before finding the operating envelope, the AJE reference geometry (SP=13 mm) has been previously optimized to operate with good efficiency in the reference operating conditions ($T_{co} = 40°C$ and $T_{ev} = 13°C$).

$$\omega_{AJE} = -0.0363 \cdot (T_{co} + 273.15) + 11.804 \quad (5)$$

Eq. (5) has been obtained using a validated Computational Fluid Dynamics (CFD) approach [27,28] that accounts for real gas effects in the working fluid (R1234yf) [33]. The RANS formulation has been adopted with the SST $k-\omega$ turbulence model and a 2D axisymmetric domain with a structured mesh of around 50,000 elements. The CFD model setup used to simulate the AJE establishes a single-phase flow hypothesis inside the jet-ejector and adiabatic walls without roughness.

- *Parabolic Trough Collector (PTC)*: This numerical model aims to assess the PTC's ability to provide thermal oil at an adequate thermal level to drive the refrigeration system ($T_{TSS} > 120\ °C$). The validated numerical model accounts for transient effects and discretizes the PTC span in spatial nodes. It is based on some literature models [34,35] and is described in detail in prior research work [28].

  Basically, the heat balance equations are solved in all the layers of the PTC line (heat transfer fluid, absorber tube, and glass envelope). The PTC constructive and performance characteristics (absorber and glass cover diameters, materials, as well as efficiency parameters) are identical to the EuroTrough model, a commercial product designed for solar concentrating applications. The only difference is the variable span assumed in the present investigation. The thermal oil Syltherm 800, a highly stable, long-lasting silicone polymer designed for high-temperature applications, has been considered as the heat transfer fluid flowing through the absorber tube.

  The following heat transfer phenomena are considered in the PTC line: (i) conduction along the PTC span in the HTF, the absorber, and the glass cover, (ii) convection between HTF and the absorber, (iii) radiation between the absorber and the glass cover, (iv) convection between the glass cover and the ambient and, (v) radiation between the glass cover and the ambient. The model has been also simplified neglecting thermal losses in the auxiliary conduction lines and the structural support and assuming that a null angle of incidence could be attained with an adequate sun-tracking system. Thus, inefficiencies associated with inadequate tilting are avoided.

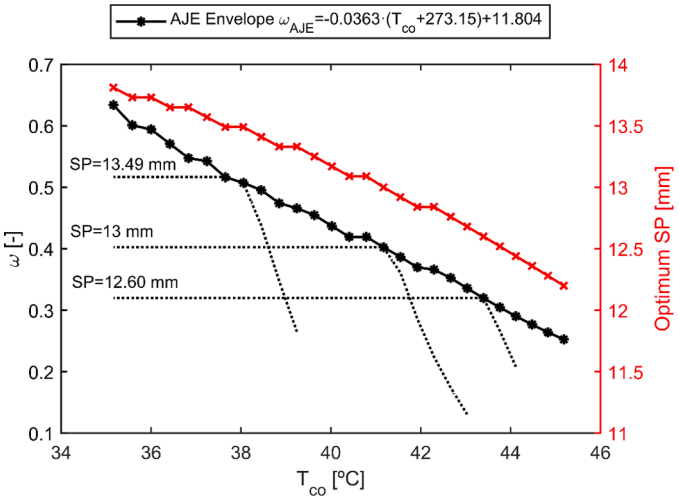

Fig. 4. Effect of the optimum spindle positioning over AJE entrainment ratio.

- *Thermal Storage System (TSS)*: The objective of the TSS model is to examine the effectiveness of a thermal energy reservoir as a mechanism to decouple the system's operation from the solar irradiance supply. In this case, as well, the numerical model consists of a nodal model with transient effects based on a thermal power balance in the TSS jacket (formed by two steel structural layers separated by a mineral wool layer). It has been formulated taking as reference the research work of Zaversky et al. [36] and considers the following heat transfer phenomena: (i) natural convection between the HTF and the internal steel layer, (ii) radiation between the HTF and the internal steel layer, (iii) conduction through the internal steel later, the mineral wool layer and the external steel layer, (iv) forced convection between the external steel layer and the ambient and, (v) radiation between the external steel layer and the ambient. For more details, the reader should refer to Galindo et al. [28]. Again, the thermal and pressure losses have been neglected in the auxiliary conduction lines.

4.2. Validation of the computational models

The validation of the computational models has been focused on two key elements: the first one is the jet-ejector, and its entrainment ratio must be accurately predicted since dramatically affects the refrigeration system performance for a given operating condition.

- In the double-choking operating mode, the entrainment ratio results predicted by the CFD approach have been contrasted with the results of Hakkaki-Fard et al. [37,38] and García del Valle et al. [39] by reproducing their jet-ejector geometries and operating conditions. Their research was dedicated to testing experimentally jet-ejector prototypes operating with R134a. The comparison is relevant in the present research since R1234yf is the new generation alternative for R134a and shows comparable thermodynamic properties. The maximum relative disparities between the present approach and the experimental results correspond to 9.3% (Hakkaki-Fard et al. [37, 38]) and 9.5% (García del Valle et al. [39]). Hence, the present CFD approach precisely predicts the response of a jet-ejector operating with a real gas model in multiple geometries and operating conditions.
- In the single-choking operating mode, the slight overestimation of the critical condensing temperature (0.6 °C) when compared to the experimental works of Shestopalov et al. [40] can be explained considering an imperfect surface finishing [41]. This manufacturing parameter is strongly influenced by the manufacturing technique and the imposition of a smooth surface carried out in the present investigation assumes a careful jet-ejector construction.

The second key element is the PTC, and its thermal energy supply is crucial for an adequate refrigeration system functioning. Fig. 5 and Fig. 6 compare the PTC outlet temperature predicted by the numerical model with the results of two different experimental campaigns [34]. In addition, the instantaneous evolution of two influential inputs, like the orientation (focusing pattern) and the power received (DNI) are presented. As can be observed, the model can capture the PTC line dynamic response with good agreement.

5. Results

This section is devoted to presenting the influence of the TSS volume factor (f), the ARS thermal power consumption ($\dot{Q}_{ge}$), and the PTC span (L_{PTC}) on the system performance from two complementary approaches: the first one analyses the instantaneous evolution of the main perfor-

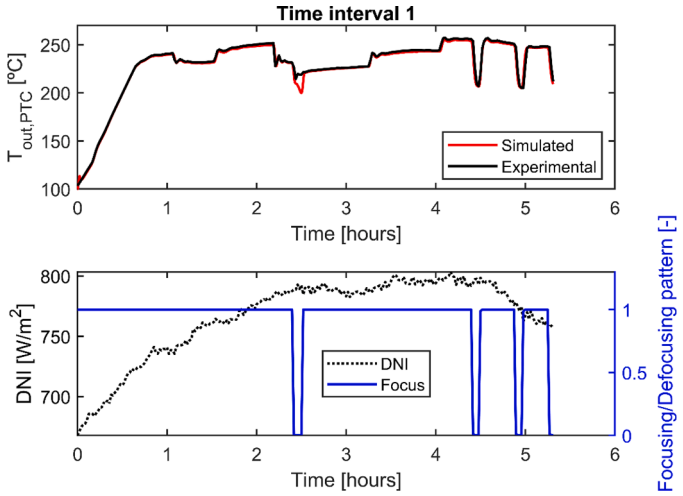

Fig. 5. Instantaneous evolution of the PTC outlet temperature for the first experimental campaign (Experimental vs computational results) and main system inputs (DNI and orientation pattern).

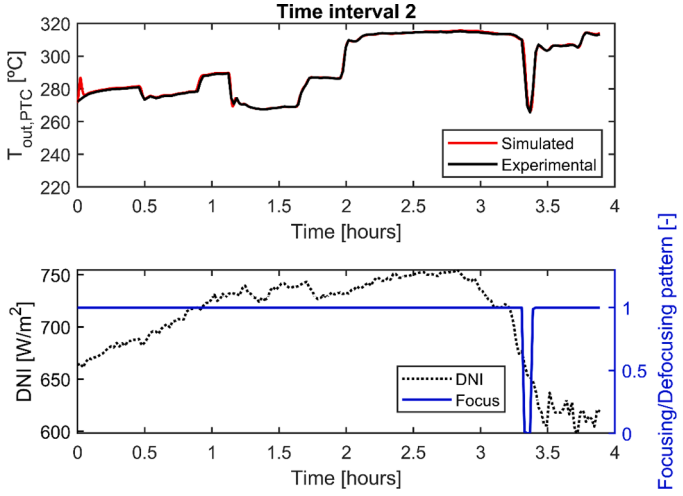

Fig. 6. Instantaneous evolution of the PTC outlet temperature for the second experimental campaign (Experimental vs computational results) and main system inputs (DNI and orientation pattern).

mance indicators over a few days. This corresponds with the short-term analysis, and it is useful to identify and understand critical situations that may negatively affect the system performance, like an increase in the ambient temperature or the appearance of clouds.

The second one, the mid-term analysis, presents averaged performance indicators along a whole warm month of the TMY. Hence, a succession of different climatic events is included. In this analysis, global and more conclusive information can be extracted to be used as design criteria. This approach has a global perspective, and it is helpful to make decisions, but it does not capture phenomena at the local scale.

5.1. Sensitivity analysis of the thermal storage system sizing: instantaneous response

5.1.1. Influence of the nominal thermal power consumption ($\dot{Q}_{ge}$)

Figs. 7 and 8 show the instantaneous evolution of the main performance indicators along three days of different dates for a constant PTC span of 7.1 m. For each figure three different nominal rates of energy consumed from the TSS ($\dot{Q}_{ge}$) for a fixed tank size ($f = 0.05$) are compared. In both analysis it is assumed that the system is initially

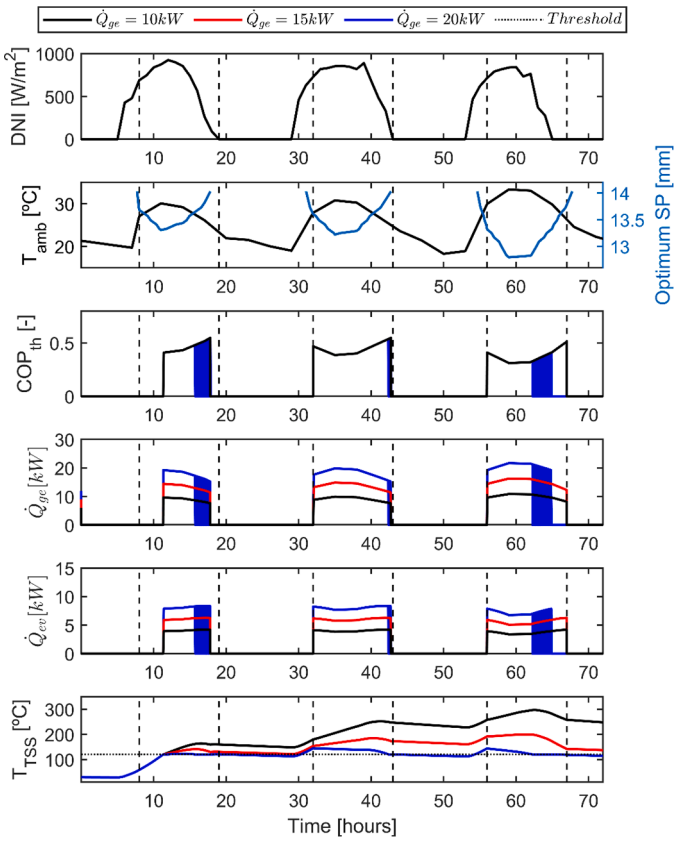

Fig. 7. Instantaneous evolution of the climatic conditions and the refrigeration system performance indicators along the days 1st-3rd of June. The collector span and the tank volume factor remain fixed ($f = 0.05$, $L_{PTC} = 7.1\ m$).

switched off, hence, the initial temperature of the PTC and the TSS corresponds with the ambient temperature. The main difference between both scenarios depicted in Fig. 7 and Fig. 8 lies in the solar irradiance profile. The first solar irradiance pattern (Fig. 7) corresponds with an almost clear-sky scenario while the second distribution (Fig. 8) is affected by occasional cloud coverage.

In the clear-sky situation, extracting a nominal thermal power of 15 kW seems to be the best strategy if priority is given to reaching a continuous operation; $\dot{Q}_{ge} = 15$ kW maximizes the refrigeration capacity without affecting the COP_{th} and the system's ability to operate continuously as can be seen in Table 1. The nominal power of 20 kW, nevertheless, causes irregular functioning. The shaded profiles marked in the figures represent an irregular functioning of the system due to the low thermal level in the tank and coincide with those time slots in which the minimum temperature threshold of 120°C in the TSS is not reached. In absence of solar irradiance during night periods, the thermal losses dominate the TSS behavior. The heat transference by convection and radiation to the ambient produce the cooling of the TSS thermal oil. If the temperature of the TSS falls below the prescribed threshold, the tank temperature must be restored in the early hours of the following day.

Nevertheless, the nominal thermal power consumption of 10 kW seems to be the most adequate in the partially cloudy scenario (Fig. 8), it guarantees a continuous operation although it exhibits a lower nominal refrigeration capacity. With an irregular solar energy reception, the nominal thermal power of 15 kW leads to a TSS discharge in the early hours of the third day. This is also reflected in Table 1 when the average COP_{th} is examined (decrease from 0.384 when $\dot{Q}_{ge} = 10$ kW to 0.342 when $\dot{Q}_{ge} = 15$ kW).

As can be observed in Figs. 7 and 8, the AJE spindle, whose displacement mechanism is reflected by the parameter SP, is

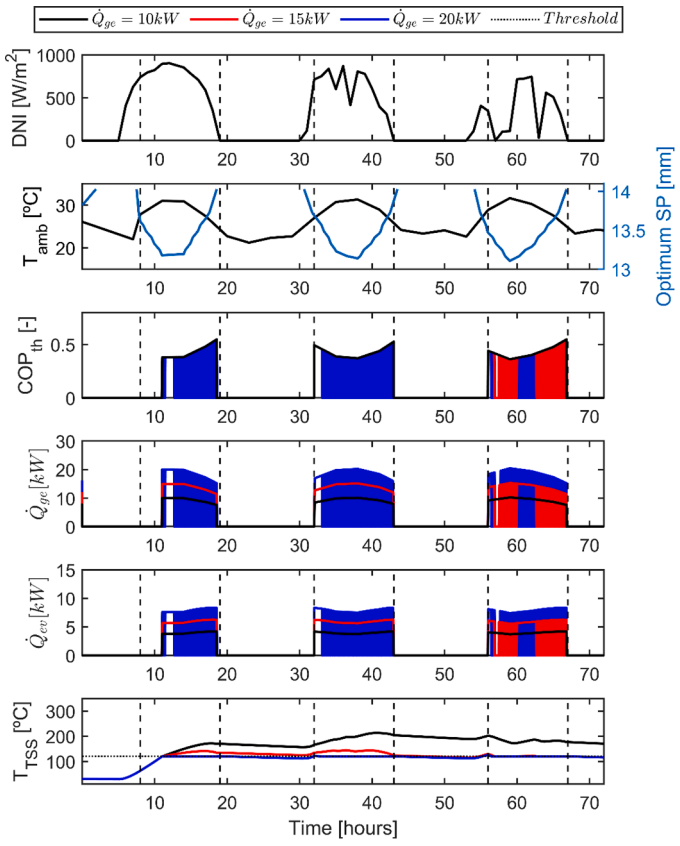

Fig. 8. Instantaneous evolution of the climatic conditions and the refrigeration system performance indicators along the days 1st-3rd of August. The collector span and the tank volume factor remain fixed ($f = 0.05$, $L_{PTC} = 7.1\ m$).

Table 1
Performance indicators averaged along three days for a fixed TSS volume factor ($f = 0.05\ m$) and collector span ($L_{PTC} = 7.1\ m$).

Case of study		$COP_{th}(average)$ [−]	$\dot{Q}_{ev}(average)$ [kW]	Activation percentage (average) [%]
Fig. 7 (1st-3rd of June)	$\dot{Q}_{ge} = 10\ kW$	0.371	3.46	88.7
	$\dot{Q}_{ge} = 15\ kW$	0.371	5.20	88.7
	$\dot{Q}_{ge} = 20\ kW$	0.312	5.88	75.7
Fig. 8 (1st-3rd of August)	$\dot{Q}_{ge} = 10\ kW$	0.384	3.58	90.4
	$\dot{Q}_{ge} = 15\ kW$	0.342	4.77	80.3
	$\dot{Q}_{ge} = 20\ kW$	0.289	5.42	68.6

continuously acting to compensate for variations in the ambient temperature. When the ambient temperature increases the spindle retracts causing an increase of the primary nozzle effective area. The spindle movement avoids the drastic performance degradation observed in a fixed-geometry jet-ejector and reduces the entrainment ratio by increasing the primary nozzle mass flow. Such operating points are characterized by lower efficiency due to higher thermal energy consumption from the thermal reservoir. The opposite effect is observed when the ambient temperature is reduced: the advancement of the spindle reduces the primary nozzle effective area, tuning the jet-ejector area ratio optimally. The result is a reduction of the mass flow rate passing through the nozzle and an efficiency improvement thanks to lower consumption of thermal energy from the TSS.

The instantaneous response of the refrigeration system provides a comprehensive description of the phenomena occurring in a limited period; however, it lacks a global perspective. In other words, the conclusions about the appropriateness of a particular system sizing are biased because they are strongly influenced by the climatic conditions of the sample days under examination. This makes it difficult to decide the most appropriate nominal power extracted from the tank ($\dot{Q}_{ge}$) and, consequently, a particular jet-ejector scale that may operate satisfactorily in multiple scenarios. Though, it anticipates that a trade-off exists, and, for a fixed storage tank size, a higher thermal power extracted from the tank would increase the system's nominal refrigeration capacity but, at the same time, it would sacrifice the system's ability to operate continuously.

5.1.2. *Influence of the hot thermal storage volume factor (f)*

An equivalent analysis could be carried out to determine the influence of different TSS volume factors (f) for a fixed nominal thermal power consumption (12 kW). Two specific scenarios showing different irradiance profiles have been analyzed. The first one (Fig. 9) covers the first 6 days of June of the TMY and it is characterized by an almost continuous solar irradiance reception except for the appearance of clouds during the 4th day. The cloudless sky found during the first three days facilitates a progressive heating-up of the TSS for all the volume factors. In the configuration with an intermediate volume ($f = 0.05$) the TSS works effectively as a heat reservoir allowing the system to face the temporary lack of thermal energy supply. Some differences in the dynamic response are distinguished for the other TSS volumes under

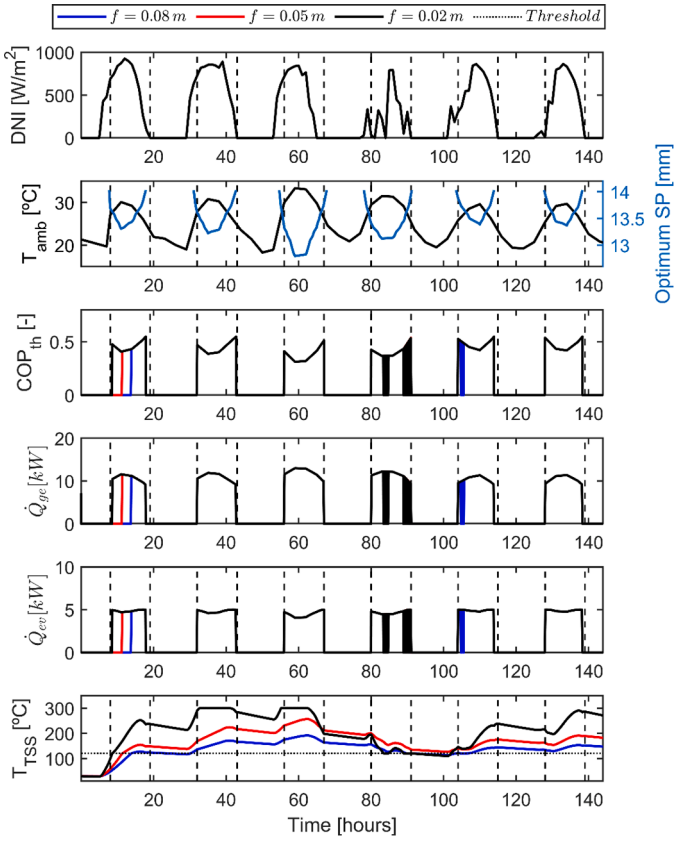

Fig. 9. Instantaneous evolution of the climatic conditions and the refrigeration system performance indicators along the days 1st −6th of June. The nominal thermal power consumed from the tank and the PTC span remain fixed ($\dot{Q}_{ge} = 12\ kW$, $L_{PTC} = 7.1\ m$).

examination. The inability of the smaller TSS ($f = 0.02$) to cope with the interruption in solar irradiance contrasts with its higher capacity to acquire rapidly the threshold thermal level after discharge events as observed, for instance, in the start-up on the 1st day and recharge at the beginning of the 5th day. Despite this, the smaller TSS shows better average performance as can be seen in Table 2. The larger TSS ($f = 0.08$), however, undergoes difficulties to acquire a high thermal level during continuous operation and discharges on the 4th day. Its high thermal inertia also affects the system negatively during the early hours of the 5th day impeding a rapid heating-up.

The second scenario covers the first six days of August of the TMY. The solar irradiance distribution is characterized by an unstable and changing behavior. As observed by monitoring the instantaneous evolution of the performance indicators (Fig. 10) and the averaged results (Table 2), the choice of small tank volumes ($f = 0.02$) clearly bring more benefits. The heating-up processes after start-up or discharge events are faster due to the lower thermal inertia of the TSS (as can be seen in the early hours after system start-up in Fig. 10). The greater storage capacity of larger tank volumes ($f = 0.05$ and $f = 0.08$) does not produce tangible benefits because the TSS does not acquire a high thermal level due to the irregular and discontinuous irradiance supply. Under this scenario, the TSS is not working as an effective thermal reservoir. What is more, the TSS with the highest volume factor ($f = 0.08$) undergoes an irregular functioning during the 3rd day and is unable to work in the late hours of the 5th day and the early hours of the 6th day. The average COP_{th} of the smallest tank (0.395), its activation percentage (97.9%) and its average refrigeration capacity (4.54 kW) suggest that the rapid heating-up is the most convenient strategy.

Again, the results are strongly influenced by the sample days under examination, and an extended analysis would shed light on the most adequate mid-term design strategy. This analysis is conducted in the following part of the study.

5.2. Sensitivity analysis of the thermal storage system sizing: month averaged response

When the instantaneous performance is averaged throughout the whole month, the performance indicators account for multiple random climatic events, hence the conclusions are more representative. Fig. 11 depicts, for different TSS volumes (f) and operating strategies ($\dot{Q}_{ge}$ nominal consumption), the main performance indicators (COP_{th}, $\dot{Q}_{ev}$ and activation percentage) averaged throughout June of the TMY.

Small TSS volumes, as well as small rates of thermal energy consumption at the TSS ($\dot{Q}_{ge}$), are preferred to maximize the COP_{th} and activation percentage, nevertheless, relatively low refrigeration capacities ($\dot{Q}_{ev}$) are found. Oppositely, a high thermal energy consumption ($\dot{Q}_{ge}$) causes frequent interruptions and COP_{th} degradation due to the TSS discharge. In contrast, the refrigeration capacity increases although the rise is less pronounced.

Table 2
Performance indicators averaged along six days for a fixed TSS thermal energy consumption ($\dot{Q}_{ge} = 12\ kW$) and PTC span ($L_{PTC} = 7.1\ m$).

Case of study		$COP_{th}(average)$ [−]	$\dot{Q}_{ev}(average)$ [kW]	Activation percentage (average) [−]
Fig. 9 (1st-6th of June)	$f = 0.02\ m$	0.418	4.60	96.5
	$f = 0.05\ m$	0.409	4.49	94.4
	$f = 0.08\ m$	0.386	4.24	89.1
Fig. 10 (1st-6th of August)	$f = 0.02\ m$	0.395	4.54	97.9
	$f = 0.05\ m$	0.368	4.23	91.6
	$f = 0.08\ m$	0.336	3.85	83.4

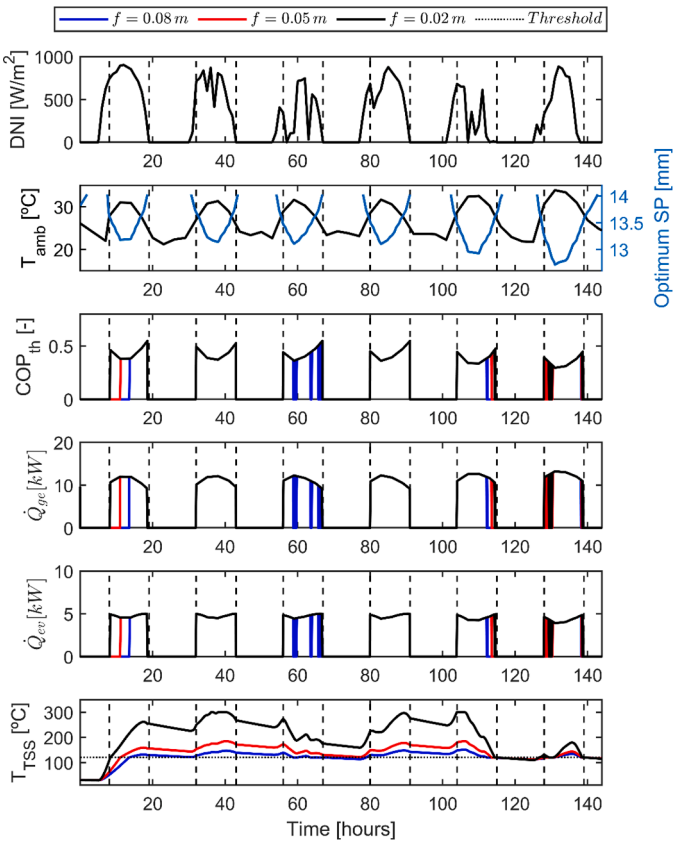

Fig. 10. Instantaneous evolution of the climatic conditions and the refrigeration system performance indicators along the days 1st −6th of August. The nominal thermal power consumed from the tank and the PTC span remain fixed ($\dot{Q}_{ge} = 12\ kW$, $L_{PTC} = 7.1\ m$).

The suitability and versatility of a particular nominal thermal power for a given tank volume would depend on the designer's criteria, and a trade-off exists:

- The TSS volume factor (f) does not have a decisive influence over the system response for a fixed rate of thermal energy consumption ($\dot{Q}_{ge}$) but small TSS volumes are preferred to reduce the thermal inertia during heating-up processes. This suggests that the TSS storage capacity losses relevance because the solar irradiance is nearly synchronized with the refrigeration needs. The benefits of larger storage capacities would be visible with other design criteria, i.e., whether the intention is to prolong the system utilization beyond the daily hours with solar irradiance. In such a case, a lower thermal energy consumption rate for the same TSS volume would allow increasing the TSS temperature, and it would act effectively as a heat reservoir. Under the prescribed requirements, there is no need to prolong the refrigeration capacity supply beyond sunny hours. Hence, the TSS's ability to act as a large heat reservoir has lower importance.
- The TSS nominal thermal power consumption ($\dot{Q}_{ge}$) greatly affects the system's dynamic response. Fig. 12 denotes the existence of an inflection point: the increase in the thermal power consumption increases the attainable refrigeration capacity with no remarkable negative impact on COP_{th} and activation percentage until a certain critical value. This critical value is suggested as the preferred design point. For the present system layout (PTC span of 7.1 m) and the

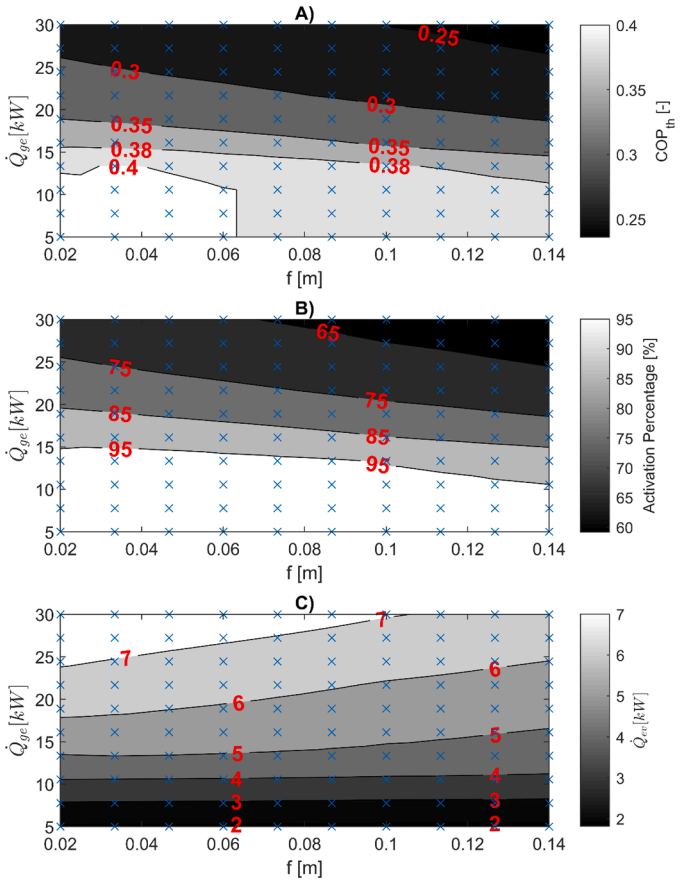

Fig. 11. Averaged COP_{th} (subfigure A), activation percentage (subfigure B) and refrigeration capacity ($\dot{Q}_{ev}$) (subfigure C) averaged along June of the TMY for different TSS volume factors (f) and nominal thermal power capacities extracted from the TSS ($\dot{Q}_{ge}$). The PTC span remains fixed ($L_{PTC} = 7.1\ m$).

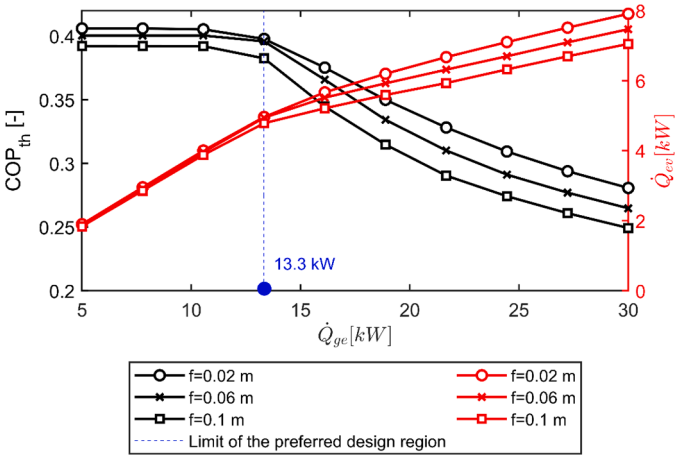

Fig. 12. Averaged COP_{th} (left axis) and refrigeration capacity (right axis) for different TSS volumes (f) and nominal thermal power consumption ($\dot{Q}_{ge}$). The PTC span remains fixed ($L_{PTC} = 7.1\ m$).

current $\dot{Q}_{ge}$ discretization scheme this value seems to be around 13.3 kW. With $\dot{Q}_{ge} > 13.3$ kW, more refrigeration capacity is produced but the greater thermal power consumption produces a faster depletion of the thermal reservoir, causing frequent interruptions in operation and averaged COP_{th} deterioration.

A comparative analysis of the system sizing with other research works is not straightforward due to the lack of standardization rules and the wide variety of applications and optimization criteria [10,11]. A fair comparison between existing facilities is quite complex. The solar collector architecture, the tank size selection, the jet-ejector design (internal geometry, refrigerant selection), or the operating conditions determined by the environment and refrigeration needs (condensing and evaporating temperatures) have a strong influence on the system response and the variability while selecting them in the literature is very heterogeneous.

Two sizing parameters ($f = V_{TSS}/A_{col}$ and $\dot{Q}_{ev}/A_{col}$) have been compared to the ones reported on comparable research works [12,16,42,43]. The former ratio ($f = V_{TSS}/A_{col}$) informs about the thermal storage system size in relation to the solar collector surface, while the latter ($\dot{Q}_{ev}/A_{col}$) informs about the refrigeration capacity in relation to the solar collector surface. The main conclusion that can be extracted is that the optimum sizing of the present research (f = 0.02 m and $\dot{Q}_{ev}/A_{col} = 0.12\ kW/m^2$) is comparable to the one reported in similar research works ($f = [0.03, 0.05]$ m and $\dot{Q}_{ev}/A_{col} = [0.07, 0.13]\ kW/m^2$) [12,16,42,43] but it is not a clear consensus or shared design rules between works.

The methodology established in this research to assess the suitability of the storage system sizing may serve as a guideline for designers of solar refrigeration plants and may be helpful to standardize the design process and the optimum sizing of the main elements.

5.3. Sensitivity analysis of the PTC span

The analysis has been extended considering several PTC spans, specifically, 5 m, 7.1 m (the baseline span selected throughout the paper), and 9 m. The already discussed volume factors have been selected also for this study: $f = 0.02$, $f = 0.05$, $f = 0.08$.

As can be observed in Fig. 13, as the PTC span increases a higher thermal power consumption from the tank ($\dot{Q}_{ge}$) is admissible without incurring in efficiency degradation. This means that the optimum strategy is to scale the refrigeration system according to the PTC span. The inflection point shown in Fig. 12 is also identified clearly in each plot of Fig. 13 and confirms the existence of a preferred design point for each PTC span. The TSS volume factor, however, shows again a lower degree of influence.

6. Practical implementation of the refrigeration system

To facilitate the operational feasibility of the system, in practice, it should be implemented together with a traditional vapor-compression refrigeration system acting as a backup. Under unfavorable climatic events, like cloudy scenarios and high ambient temperatures, the jet-ejector refrigeration system might be unable to operate. The inactivity periods are reflected in all the scenarios studied by the activation percentage, which is in most of the cases below 100%. Besides, the continuous adjustment of the jet-ejector spindle following the changes in the ambient temperature enhances or deteriorates the system efficiency in comparison with the nominal or design conditions as seen in Figs. 7, 8, 9, and 10. This makes it difficult to maintain a fixed rated refrigeration load since the refrigeration load delivered is coupled with the ambient temperature. The auxiliary traditional refrigeration system might be also helpful to complement the refrigeration capacity that the jet-ejector refrigeration system cannot deliver.

In addition to backup systems, the jet-ejector refrigeration system itself should implement control laws and mechanical actuators to regulate the jet-ejector spindle position according to the instantaneous ambient conditions. On the solar field side, the thermal oil recirculation and the orientation of the receiver should be controlled according to the thermal storage system temperature and the irradiance conditions. The intention would be to manage the temperature of the thermal oil inside

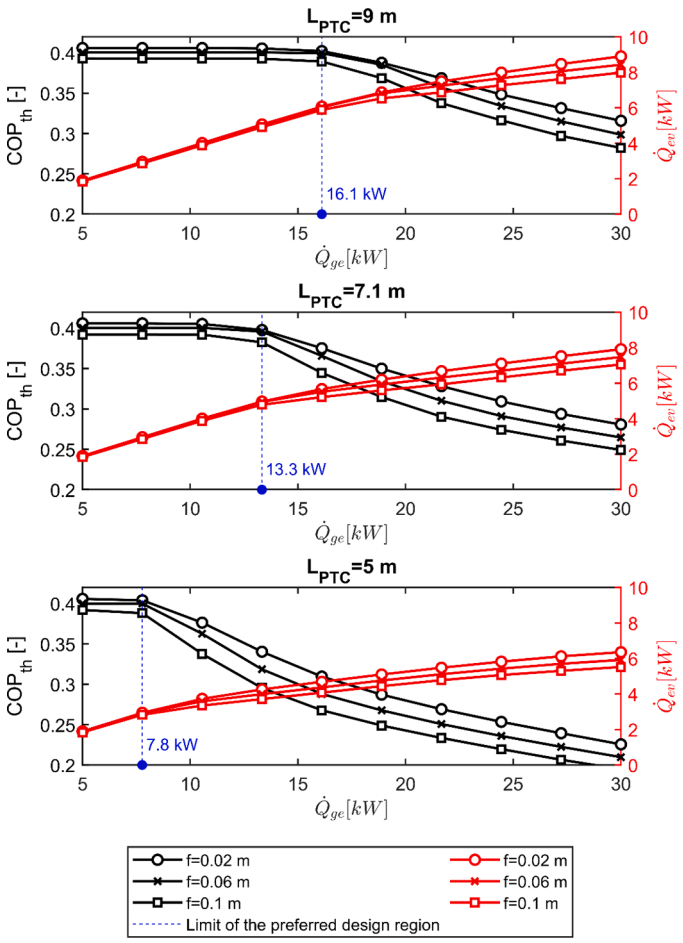

Fig. 13. Averaged COP_{th} (left axis) and refrigeration capacity (right axis) for different TSS volumes (f), nominal thermal power consumption ($\dot{Q}_{ge}$) and different PTC spans. The PTC span of 7.1 m corresponds with the reference layout examined throughout the research work.

the tank smartly, defocusing the receiver when the temperature is too high and implementing a two-axis solar tracker to guarantee an optimum orientation when a heating up of the tank is required. In the latter scenario, it might be necessary to interrupt the thermal oil supply to the generator when the thermal level is insufficient or maintain it when the thermal oil temperature is sufficient to drive the system.

For practical implementation, the thermoeconomic analysis would be crucial. Since the solar collector and the thermal storage system are the costlier elements, a smart integration with existing solar heating installations would revalue the refrigeration concept and would contribute to a financially sustainable system.

7. Conclusions

In this work, different strategies for sizing and managing a thermal storage system for a solar-assisted jet-ejector refrigeration system are presented. The refrigeration system is intended to operate intensively between the hour interval ranging between 08:00 and 19:00 during the warm months in a Mediterranean climate.

Focusing the analysis on the timespan of hours or few days lead to partial and incomplete results, making it difficult to draw general findings due to the strong influence of particular climatic events. Notwithstanding, this analysis is helpful to understand the system's instantaneous response and its deficiencies.

If an overall month is assessed generalized results can be extracted from the overall averaged figures. A trade-off between the three competing performance indicators has been found, namely, (i) the refrigeration system efficiency (COP_{th}), (ii) the refrigeration capacity ($\dot{Q}_{ev}$), and (iii) the system's capability to operate without interruptions. For a given collector surface and tank size, it has been demonstrated that there is an upper thermal power consumption limit below which the refrigeration system can operate almost continuously preserving a high efficiency. This inflection point and its vicinity represent the preferred design region. For example, for a PTC span of 7.1 m, a nominal thermal power of 13.3 kW offers the best compromise between achievable COP_{th}, refrigeration capacity and system's ability to remain in operation ensuring an adequate management of the storage tank. A higher thermal energy consumption would improve the refrigeration capacity in some time slots but it would be detrimental to the system's efficiency and its ability to operate without interruptions.

Unlike the thermal energy consumption strategy, the tank size and, therefore, its storage capacity is less decisive because in this application the system is intended to operate in a time slot with solar irradiance supply (08:00–19:00). For this scenario, small thermal storage volumes are preferred to achieve rapid heating-up after discharge events.

CRediT authorship contribution statement

José Manuel Luján: Resources, Project administration, Supervision, Funding acquisition. **José Galindo:** Conceptualization, Funding acquisition, Project administration, Supervision. **Vicente Dolz:** Methodology, Investigation, Visualization, Writing – original draft. **Alberto Ponce-Mora:** Software, Investigation, Validation, Visualization, Writing – original draft.

Declaration of Competing Interest

The authors declare that they have no known competing financial interests or personal relationships that could have appeared to influence the work reported in this paper entitled "Optimization of the thermal storage system in a solar-driven refrigeration system equipped with an adjustable jet-ejector".

Acknowledgments

Authors want to acknowledge to the institution "Conselleria d'Innovació, Universitats, Ciència i Societat Digital de la Generalitat Valenciana" for the public aid granted in the research project AICO/2021/124).

References

[1] N. Kalkan, E.A. Young, A. Celiktas, Solar thermal air conditioning technology reducing the footprint of solar thermal air conditioning, Renew. Sustain. Energy Rev. 16 (2012) 6352–6383, https://doi.org/10.1016/j.rser.2012.07.014.
[2] B. Tashtoush, Y. Nayfeh, Energy and economic analysis of a variable-geometry ejector in solar cooling systems for residential buildings, J. Energy Storage 27 (2020), 101061, https://doi.org/10.1016/j.est.2019.101061.
[3] L.A. Chidambaram, A.S. Ramana, G. Kamaraj, R. Velraj, Review of solar cooling methods and thermal storage options, Renew. Sustain. Energy Rev. 15 (2011) 3220–3228, https://doi.org/10.1016/j.rser.2011.04.018.
[4] R.P. Singh, J.Y. Sze, S.C. Kaushik, D. Rakshit, A. Romagnoli, Thermal performance enhancement of eutectic PCM laden with functionalised graphene nanoplatelets for an efficient solar absorption cooling storage system, J. Energy Storage 33 (2021), 102092, https://doi.org/10.1016/j.est.2020.102092.
[5] H.J. Xu, C.Y. Zhao, Thermal performance of cascaded thermal storage with phase-change materials (PCMs). Part I: steady cases, Int. J. Heat Mass Transf. 106 (2017) 932–944, https://doi.org/10.1016/j.ijheatmasstransfer.2016.10.054.
[6] I. Sarbu, C. Sebarchievici, A comprehensive review of thermal energy storage, Sustain (2018) 10, https://doi.org/10.3390/su10010191.
[7] A.A. Al-Abidi, S. Bin Mat, K. Sopian, M.Y. Sulaiman, C.H. Lim, A. Th, Review of thermal energy storage for air conditioning systems, Renew. Sustain. Energy Rev. 16 (2012) 5802–5819, https://doi.org/10.1016/j.rser.2012.05.030.
[8] K.S. Reddy, V. Mudgal, T.K. Mallick, Review of latent heat thermal energy storage for improved material stability and effective load management, J. Energy Storage 15 (2018) 205–227, https://doi.org/10.1016/j.est.2017.11.005.
[9] H.J. Xu, C.Y. Zhao, Analytical considerations on optimization of cascaded heat transfer process for thermal storage system with principles of thermodynamics,

Renew. Energy 132 (2019) 826–845, https://doi.org/10.1016/j.renene.2018.07.135.
[10] S. Pintaldi, C. Perfumo, S. Sethuvenkatraman, S. White, G. Rosengarten, A review of thermal energy storage technologies and control approaches for solar cooling, Renew. Sustain. Energy Rev. 41 (2015) 975–995, https://doi.org/10.1016/j.rser.2014.08.062.
[11] Sparber, B.W., Napolitano, A., Eckert, G., Preisler, A., Task 38, Solar Air-Conditioning and Refrigeration: State of the art of existing solar heating and cooling systems, 2009.
[12] B. Tashtoush, A. Alshare, S. Al-Rifai, Hourly dynamic simulation of solar ejector cooling system using TRNSYS for Jordanian climate, Energy Convers. Manag. 100 (2015) 288–299, https://doi.org/10.1016/j.enconman.2015.05.010.
[13] S. Rosiek, F.J. Batlles, Integration of the solar thermal energy in the construction: analysis of the solar-assisted air-conditioning system installed in CIESOL building, Renew. Energy 34 (2009) 1423–1431, https://doi.org/10.1016/j.renene.2008.11.021.
[14] M. Qu, H. Yin, D.H. Archer, A solar thermal cooling and heating system for a building: experimental and model based performance analysis and design, Sol. Energy 84 (2010) 166–182, https://doi.org/10.1016/j.solener.2009.10.010.
[15] A. Syed, M. Izquierdo, P. Rodríguez, G. Maidment, J. Missenden, A. Lecuona, R. Tozer, A novel experimental investigation of a solar cooling system in Madrid, Int. J. Refrig. 28 (2005) 859–871, https://doi.org/10.1016/j.ijrefrig.2005.01.007.
[16] V. Van Nguyen, S. Varga, J. Soares, V. Dvorak, A.C. Oliveira, Applying a variable geometry ejector in a solar ejector refrigeration system, Int. J. Refrig. 113 (2020) 187–195, https://doi.org/10.1016/j.ijrefrig.2020.01.018.
[17] D.S. Kim, C.A. Infante Ferreira, Solar refrigeration options - a state-of-the-art review, Int. J. Refrig. 31 (2008) 3–15, https://doi.org/10.1016/j.ijrefrig.2007.07.011.
[18] G. Besagni, F. Inzoli, Computational fluid-dynamics modeling of supersonic ejectors: screening of turbulence modeling approaches, Appl. Therm. Eng. 117 (2017) 122–144, https://doi.org/10.1016/j.applthermaleng.2017.02.011.
[19] M. Dennis, K. Garzoli, Use of variable geometry ejector with cold store to achieve high solar fraction for solar cooling, Int. J. Refrig. 34 (2011) 1626–1632, https://doi.org/10.1016/j.ijrefrig.2010.08.006.
[20] B.M. Diaconu, S. Varga, A.C. Oliveira, Numerical simulation of a solar-assisted ejector air conditioning system with cold storage, Energy 36 (2011) 1280–1291, https://doi.org/10.1016/j.energy.2010.11.015.
[21] S. Varga, P.M.S. Lebre, A.C. Oliveira, CFD study of a variable area ratio ejector using R600a and R152a refrigerants, Int. J. Refrig. 36 (2013) 157–165, https://doi.org/10.1016/j.ijrefrig.2012.10.016.
[22] S. Varga, A.C. Oliveira, X. Ma, S.A. Omer, W. Zhang, S.B. Riffat, Experimental and numerical analysis of a variable area ratio steam ejector, Int. J. Refrig. 34 (2011) 1668–1675, https://doi.org/10.1016/j.ijrefrig.2010.12.020.
[23] Z. Chen, X. Jin, A. Shimizu, E. Hihara, C. Dang, Effects of the nozzle configuration on solar-powered variable geometry ejectors, Sol. Energy 150 (2017) 275–286, https://doi.org/10.1016/j.solener.2017.04.017.
[24] L. Wang, J. Liu, T. Zou, J. Du, F. Jia, Auto-tuning ejector for refrigeration system, Energy 161 (2018) 536–543, https://doi.org/10.1016/j.energy.2018.07.110.
[25] G. Besagni, R. Mereu, F. Inzoli, Ejector refrigeration: a comprehensive review, Renew. Sustain. Energy Rev. 53 (2016) 373–407, https://doi.org/10.1016/j.rser.2015.08.059.
[26] J. Chen, S. Jarall, H. Havtun, B. Palm, A review on versatile ejector applications in refrigeration systems, Renew. Sustain. Energy Rev. 49 (2015) 67–90, https://doi.org/10.1016/j.rser.2015.04.073.
[27] J. Galindo, V. Dolz, L.M. García-Cuevas, A. Ponce-Mora, Numerical evaluation of a solar-assisted jet-ejector refrigeration system: screening of environmentally friendly refrigerants, Energy Convers. Manag. 210 (2020), 112681, https://doi.org/10.1016/j.enconman.2020.112681.
[28] J. Galindo, V. Dolz, A. Tiseira, A. Ponce-Mora, Numerical assessment of the dynamic behavior of a solar-driven jet-ejector refrigeration system equipped with an adjustable jet-ejector, Int. J. Refrig. 121 (2021) 168–182, https://doi.org/10.1016/j.ijrefrig.2020.10.019.
[29] R.H. Yen, B.J. Huang, C.Y. Chen, T.Y. Shiu, C.W. Cheng, S.S. Chen, K. Shestopalov, Performance optimization for a variable throat ejector in a solar refrigeration system, Int. J. Refrig. 36 (2013) 1512–1520, https://doi.org/10.1016/j.ijrefrig.2013.04.005.
[30] B. Gil, J. Kasperski, Efficiency analysis of alternative refrigerants for ejector cooling cycles, Energy Convers. Manag. 94 (2015) 12–18, https://doi.org/10.1016/j.enconman.2015.01.056.
[31] M.C. Rodríguez-Hidalgo, P.A. Rodríguez-Aumente, A. Lecuona, M. Legrand, R. Ventas, Domestic hot water consumption vs. solar thermal energy storage: the optimum size of the storage tank, Appl. Energy 97 (2012) 897–906, https://doi.org/10.1016/j.apenergy.2011.12.088.
[32] J. Galindo, V. Dolz, A. Tiseira, A. Ponce-Mora, Thermodynamic Analysis and Optimization of a Jet Ejector Refrigeration Cycle Used To Cool Down the Intake Air in an Ic Engine, Int. J. Refrig. 103 (2019) 253–263, https://doi.org/10.1016/j.ijrefrig.2019.04.019.
[33] M. Richter, M.O. McLinden, E.W. Lemmon, Thermodynamic properties of 2,3,3,3-tetrafluoroprop-1-ene (R1234yf): vapor pressure and p - φ - T measurements and an equation of state, J. Chem. Eng. Data 56 (2011) 3254–3264, https://doi.org/10.1021/je200369m.
[34] A. Desideri, R. Dickes, J. Bonilla, L. Valenzuela, S. Quoilin, V. Lemort, Steady-state and dynamic validation of a parabolic trough collector model using the ThermoCycle modelica library, Sol. Energy 174 (2018) 866–877, https://doi.org/10.1016/j.solener.2018.08.026.
[35] T. Fasquelle, Q. Falcoz, P. Neveu, F. Lecat, G. Flamant, A thermal model to predict the dynamic performances of parabolic trough lines, Energy 141 (2017) 1187–1203, https://doi.org/10.1016/j.energy.2017.09.063.
[36] F. Zaversky, J. García-Barberena, M. Sánchez, D. Astrain, Transient molten salt two-tank thermal storage modeling for CSP performance simulations, Sol. Energy 93 (2013) 294–311, https://doi.org/10.1016/j.solener.2013.02.034.
[37] A. Hakkaki-Fard, Z. Aidoun, M. Ouzzane, A computational methodology for ejector design and performance maximisation, Energy Convers. Manag. 105 (2015) 1291–1302, https://doi.org/10.1016/j.enconman.2015.08.070.
[38] A. Hakkaki-Fard, M. Poirier, Z. Aidoun, M. Ouzzane, D. Giguère, An experimental study of ejectors supported by CFD, Refrig. Sci. Technol. (2015) 2030–2037, https://doi.org/10.18462/iir.icr.2015.0609.
[39] J. García Del Valle, J.M. Saíz Jabardo, F. Castro Ruiz, J.F. San José Alonso, An experimental investigation of a R-134a ejector refrigeration system, Int. J. Refrig. 46 (2014) 105–113, https://doi.org/10.1016/j.ijrefrig.2014.05.028.
[40] K.O. Shestopalov, B.J. Huang, V.O. Petrenko, O.S. Volovyk, Investigation of an experimental ejector refrigeration machine operating with refrigerant R245fa at design and off-design working conditions. Part 2. Theoretical and experimental results, Int. J. Refrig. 55 (2015) 212–223, https://doi.org/10.1016/j.ijrefrig.2015.02.004.
[41] F. Mazzelli, A. Milazzo, Performance analysis of a supersonic ejector cycle working with R245fa, Int. J. Refrig. 49 (2015) 79–92, https://doi.org/10.1016/j.ijrefrig.2014.09.020.
[42] W. Pridasawas, P. Lundqvist, A year-round dynamic simulation of a solar-driven ejector refrigeration system with iso-butane as a refrigerant, Int. J. Refrig. 30 (2007) 840–850, https://doi.org/10.1016/j.ijrefrig.2006.11.012.
[43] H. Vidal, S. Colle, G.D.S. Pereira, Modelling and hourly simulation of a solar ejector cooling system, Appl. Therm. Eng. 26 (2006) 663–672, https://doi.org/10.1016/j.applthermaleng.2005.09.012.